An Energy-Efficient ADO-OFDM System for Optical Wireless Communication

Wei-Wen Hu, *Member, IEEE*

***Abstract*—This paper proposes an energy-efficient asymmetrically clipped direct-current (DC) biased optical orthogonal frequency division multiplexing (EEADO-OFDM) scheme, which replaces the fixed DC bias of DC biased optical OFDM (DCO-OFDM) branch with a adaptive DC bias for optical wireless communications. In the EEADO-OFDM, an adaptive DC bias is dynamically designed according to amplitude of DCO-OFDM signal samples to enhance the power efficiency. After superimposing the obtained DC bias on the original DCO-OFDM signal, the resultant DCO-OFDM signal is non-negative and further ensure that a non-negative EEADO-OFDM signal is produced by directly combining DCO-OFDM signal with the clipped asymmetrically clipped optical OFDM (ACO-OFDM) signal. In particular, the interference caused by the obtained DC bias is proved to fall on even subcarriers only, which implies that the interference can be modulated on the partial odd subcarriers of ACO-OFDM branch. Afterward, we could use conventional ACO-OFDM receiver to demodulate the adopted odd subcarriers for the detection of interference. Simulation results show that, under the equal optical power constraints, the proposed EEADO-OFDM achieves no error floors of bit error rate compared with the ADO-OFDM, thus indicating that the clipping noise is always negligible in EEADO-OFDM.**

***Index Terms*—ADO-OFDM, DCO-OFDM, direct current, Hermitian symmetry.**

I. Introduction

RECENTLY, optical wireless communication (OWC) has received increasing attention in many wireless applications such as indoor broadcasting, indoor positioning, and outdoor vehicle-to-vehicle communication [1], [2]. Compared with the radio frequency based transmission, OWC has the superiority in license-free spectrum, high security and no electromagnetic interference. For OWC systems, intensity modulation and direct detection is applied in optical signals indicating that the amplitude of signal has to be the real and non-negative. Moreover, orthogonal frequency division multiplexing (OFDM) is the most used modulation scheme, which possess the advantage of single one-tap equalization and the capability of resisting inter-symbol interference [3].

Up to now, several different OFDM schemes can be classified into two major categories, where the first one is non direct current biased (DC-biased) method [4], [5], [6], [7], [8], [9], [10] and the second one is DC-biased method [12], [13], [14], [15], [16]. Non DC-biased methods mean that no extra DC bias is required at the transmitter side, such as Filp-OFDM [4], asymmetrically clipped optical OFDM (ACO-OFDM) [5], clipping-enhancement polarity-header optical OFDM (CE-PHO-OFDM) [6], polar OFDM (P-OFDM) [7], U-OFDM [8] and layer ACO-OFDM (LACO-OFDM) [9], [10], [11]. However, the most non DC-biased methods are inefficient in terms of spectrum efficiency because only half of the subcarriers are used in ACO-OFDM and double frame duration are required in Filp-OFDM, CE-PHO-OFDM, P-OFDM, and U-OFDM. Recently, layered ACO-OFDM (LACO-OFDM) is proposed in [9], [10], [11] by combining different layers of ACO-OFDM signals to improve the spectrum efficiency. However, the receiver of LACO-OFDM incurs high computational complexity and processing latency using a large number of layers. Alternatively, DC-biased optical OFDM (DCO-OFDM) scheme has been proposed to improve the spectrum efficiency at the cost of power efficiency. In DCO-OFDM, a fixed DC bias is introduced to superimpose on the bipolar signals to make the signals non-negative which indicates that the performance of DCO-OFDM highly depends on the added DC bias [12], [13], [14], [15]. When the added DC bias is too large, it makes the DCO-OFDM inefficient in terms of the optical power. On the other hand, small DC bias will lead to the introduction of clipping distortion at the transmitter and further result in bit error rate (BER) graphs plateau [16]. To provide both spectrum and power efficiency simultaneously, an asymmetrical clipped DC biased optical OFDM (ADO-OFDM) was proposed by combining both the ACO-OFDM and the DCO-OFDM concepts [17], [18], [19], [20]. Although the spectrum efficiency and optical power efficiency of ADO-OFDM is better than ACO-OFDM and DCO-OFDM, respectively, ADO-OFDM still suffers from the same drawbacks of aforementioned DC-biased methods. For example, when the added DC bias is small or the adopted constellation sizes are large, the clipping noise is introduced. Raising the DC bias can decrease clipping noise but at the detriment of power efficiency.

In this paper, an energy-efficient asymmetrically clipped DC biased optical OFDM (EEADO-OFDM) scheme is conceived for the OWC systems, where a adaptive DC bias is designed according to amplitude of DCO-OFDM signal. The obtained DC bias is superimposed to the original DCO-OFDM signal to guarantee the non-negativity of DCO-OFDM signal further resulting in EEADO-OFDM signals have also non-negative amplitudes. Moreover, we prove that the interference caused by the introduced DC bias falls on the even subcarriers only,

Manuscript received 28 October 2023; accepted 2 November 2023. Date of publication 6 November 2023; date of current version 22 November 2023. This work was supported by the National Science and Technology Council, Taiwan, under Grant NSTC 112-2221-E-150-019.

The author is with the Department of Electrical Engineering, National Formosa University, Huwei 632, Taiwan (e-mail: huweiwen1106@gmail.com).

Digital Object Identifier 10.1109/JPHOT.2023.3330642

indicating that the interference could be mapped and modulated on the the odd subcarriers of ACO-OFDM branch, which means the detection of interference can be processed by using a standard ACO-OFDM receiver. Moreover, the numerical analysis of spectral efficiency, optical power, BER, and computational complexity of the EEADO-OFDM is also presented. Simulation results show that the EEADO-OFDM exhibits no error floors of BER at the cases of high-order modulation schemes and low dc bias compared to the conventional ADO-OFDM.

The rest of the paper is organized as follows. Section II gives the brief introduction for conventional ADO-OFDM. Section III describes the system model of EEADO-OFDM including transmitter and receiver. In Section IV, we give theoretical analysis of computational complexity, BER, optical power and spectral efficiency for the EEADO-OFDM system. We compare the EEADO-OFDM with ADO-OFDM and the existing DC-biased optical OFDM systems in terms of BER in Section V. Finally, Section VI concludes the paper.

II. Overview of Conventional ADO-OFDM

In this section, the transmitter and receiver of the conventional ADO-OFDM are briefly demonstrated. For the transmitter of ADO-OFDM, odd subcarriers are occupied by the ACO-OFDM symbols while even subcarriers are used by the DCO-OFDM signals. After applying the Hermitian symmetry on the modulated symbols, the frequency-domain DCO-OFDM signals can be written as

$$\mathbf{X}=\left[0,0,X_2,0,\ldots,X_{\frac{N}{2}-2},0,0,0,X^*_{\frac{N}{2}-2},\ldots,0,X^*_2,0\right], \tag{1}$$

where X_k denotes the kth complex-valued quadrature amplitude modulation (QAM) modulated symbol with a zero mean and a variance of $\sigma_X^2 = E[|X_k|^2]$. $E[\cdot]$ denotes the expectation operation. The adopted constellation size in DCO-OFDM branch is set to be M_e. Then, the time-domain DCO-OFDM signals can be obtained after the operation of N-point IFFT, which are given by

$$x_n = \frac{1}{\sqrt{N}}\sum_{k=0}^{N-1} X_k e^{j\frac{2\pi kn}{N}}, \quad 0\le n\le N-1 \tag{2}$$

where x_n has a zero mean and a variance of $\sigma_x^2 = E[|x_n|^2] = \sigma_X^2/2$. To satisfy the non-negative property, a DC bias is added to x_n and is formulated as $B_{DC,DCO} = u\sqrt{E[|x_n|^2]} = u\sigma_x$, where u is a proportional constant. In general, the bias level in dB is defined as $10\log_{10}(u^2+1)$. Finally, the transmitted signals of DCO-OFDM branch are obtained by clipping the remaining negative part of $x_n + B_{DC,DCO}$, which are given by

$$x_{n,DCO} = \begin{cases} x_n + B_{DC,DCO}, & x_n + B_{DC,DCO} \ge 0 \\ 0, & x_n + B_{DC,DCO} < 0 \end{cases} \tag{3}$$

In addition, the frequency-domain ACO-OFDM signals can be written as

$$\mathbf{Y}=\left[0,Y_1,0,Y_3,\ldots,Y_{\frac{N}{2}-1},0,Y^*_{\frac{N}{2}-1},\ldots,Y^*_1\right], \tag{4}$$

where Y_k denotes the kth complex-valued QAM modulated symbols with a zero mean and a variance of $\sigma_Y^2 = E[|Y_k|^2]$.

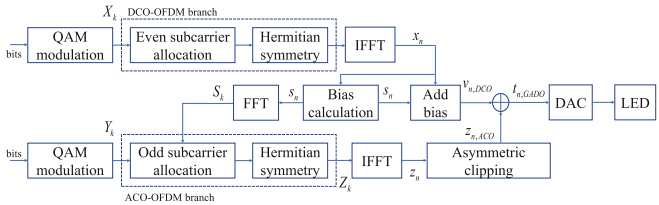

Fig. 1. Transmitter of the EEADO-OFDM.

The adopted constellation size in ACO-OFDM branch is set to be M_o. After the process of N-point IFFT, the time-domain ACO-OFDM signals can be obtained as

$$y_n = \frac{1}{\sqrt{N}}\sum_{k=0}^{N-1} Y_k e^{j\frac{2\pi kn}{N}}, \quad 0\le n\le N-1 \tag{5}$$

where y_n has a zero mean and a variance of $\sigma_y^2 = E[|y_n|^2] = \sigma_Y^2/2$. Unlike DCO-OFDM branch, the unipolar ACO-OFDM signals are obtained by clipping the remaining negative part of y_n, which are given by

$$y_{n,ACO} = \begin{cases} y_n, & y_n \ge 0 \\ 0, & y_n < 0 \end{cases} \tag{6}$$

Combining ACO-OFDM signals with DCO-OFDM signals, the transmitted ADO-OFDM signals can be formulated by

$$t_{n,ADO} = y_{n,ACO} + x_{n,DCO}, \quad 0\le n\le N-1 \tag{7}$$

Considering the LED nonlinearity, the ADO-OFDM signal can be expressed as

$$t_{n,ADO}^{clip} = \begin{cases} \varepsilon_{upper}, & t_{n,ADO} > \varepsilon_{upper}, \\ t_{n,ADO}, & 0 \le t_{n,ADO} \le \varepsilon_{upper}, \\ 0, & t_{n,ADO} < 0, \end{cases} \tag{8}$$

where ε_{upper} denotes the maximum permissible voltage.

At the receiver side, the received optical signals are firstly converted into the electrical signals using a photodetector. Then, the received electrical signals pass through the process of removing the cyclic prefix and FFT operation. The resultant ACO-OFDM symbols on odd subcarriers can be estimated by conventional ACO-OFDM receiver. After that, time-domain ACO-OFDM signals can be regenerated and subtracted from the received signals. The DCO-OFDM symbols from even subcarriers could be estimated after the interference cancellation procedure [17].

III. System Model of EEADO-OFDM

A. The Block Diagram of EEADO-OFDM Transmitter

The block diagram of the EEADO-OFDM transmitter is depicted in Fig. 1. Similar to ADO-OFDM, even subcarriers are used for the modulation of DCO-OFDM, which means that time-domain DCO-OFDM signals for EEADO-OFDM can be obtained by (2). Instead of adding a fixed DC bias to x_n, the DC bias of the EEADO-OFDM system is determined by flexible bias calculation as follows. Firstly, x_n is divided into I disjoint subblocks, where each subblock contains $G = N/I$ time-domain samples. It is assumed that both N and I are

non-negative integer powers of two, indicating that I must be a divisor of N so that G is an integer. Accordingly, the gth time-domain sample of ith subblock, $x_{i,g}$, can be represented as

$$x_{i,g} = x_n, \quad n = g + iG, \tag{9}$$

where $0 \le i \le I-1$ and $0 \le g \le G-1$. Let m_g be the minimum values of gth sample among I subblocks, that is,

$$\begin{aligned} m_g &= \arg \min_{0 \le i \le I-1} x_{i,g} \\ &= \arg \min \left\{ x_{0,g}, x_{1,g} \ldots, x_{I,g} \right\}, 0 \le g \le G-1 \end{aligned} \tag{10}$$

On the basis of (10), we could construct a time-domain sequence $\mathbf{s} = \{s_n\}_{n=0}^{N-1}$ by concatenating m_g with I times as follows

$$\begin{aligned} \mathbf{s} &= \{s_n\}_{n=0}^{N-1} \\ &= \left\{ \underbrace{m_0, m_1, \ldots, m_{G-1}, \ldots, m_0, m_1, \ldots, m_{G-1}}_{I \text{ times}} \right\} \end{aligned} \tag{11}$$

Further from (10), it can be seen that if the gth samples of all $x_{i,g}$ are positive, the minimum value is positive. If one of the gth samples of all $x_{i,g}$ is negative, the minimum value is negative. Based on these observations, we can generate the non-negative real samples $v_{n,DCO}$ as follows

$$v_{n,DCO} = x_n + s_n = \begin{cases} x_{i,g}, & m_g \ge 0 \\ x_{i,g} - m_g, & m_g < 0 \end{cases} \tag{12}$$

Equation (12) indicates that if $m_g \ge 0$, no DC bias is required, leading to $m_g = 0$. On the other hand, it can be found that the non-negativity of the gth time-domain sample of ith subblock could be guaranteed by subtracting the m_g from the $x_{i,g}$ when $m_g < 0$. Obviously, $\mathbf{s}$ has the structure of

$$m_g = m_{g+G} = m_{g+2\,G} = \ldots = m_{g+(I-1)G}, \tag{13}$$

where $0 \le g \le G-1$. Performing FFT on $\mathbf{s}$ yields

$$S_k = \begin{cases} 0, & k \in \text{odd} \\ 0, & k = It + 2l \\ \frac{I}{\sqrt{N}} \sum_{g=0}^{G-1} m_g e^{-j\frac{2\pi g t}{G}}, & k = It \end{cases} \tag{14}$$

where $0 \le t \le N/I - 1$ and $1 \le l \le I/2 - 1$. The detailed proof is provided in the Appendix. According to (14), we notice that the added time-domain sequences $\mathbf{s}$ have the frequency-domain non-zero values only at the 0th, Ith,..., $(N-I)$th subcarriers, indicating that the number of non-zero values of $\mathbf{S} = \{S_k\}_{k=0}^{N-1}$ are N/I. It also means that the interference generated by $\mathbf{s}$ only imposes on the even subcarriers. Therefore, we modulate these non-zero values on the partial odd subcarriers of ACO-OFDM branch and then uses the conventional ACO-OFDM receiver to estimate the non-zero values. Afterward, the interference on the even subcarriers caused from $\mathbf{s}$ could be directly removed by subtracting $\mathbf{s}$ from the received signals on even subcarriers.

Excluding the 0th subcarrier and considering the Hermitian symmetry operation, the required number of odd subcarriers for modulating of S_k are $N_{int} = N/(2I)$. Unlike ACO-OFDM branch of conventional ADO-OFDM, the complex-valued symbols $\mathbf{Z} = \{Z_k\}_{k=0}^{N-1}$ modulated on the odd subcarriers

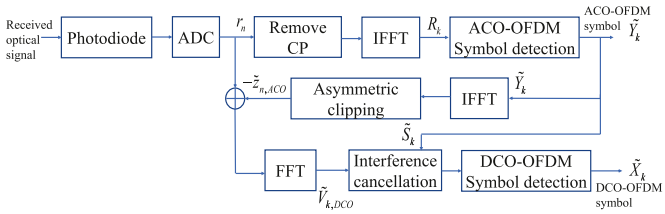

Fig. 2. Receiver of the EEADO-OFDM.

in EEADO-OFDM system are given by

$$Z_k = \begin{cases} S_k, & k = 1, 3, \ldots, 2N_{int} - 1 \\ Y_k, & k = 2N_{int} + 1, 2N_{int} + 3, \ldots, N/2 - 1 \end{cases} \tag{15}$$

where the S_k comes from the non-zero values derived in (14). The corresponding time-domain signals after Hermitian symmetry and IFFT operations can be represented as

$$z_n = \frac{1}{\sqrt{N}} \sum_{k=0}^{N-1} Z_k e^{j\frac{2\pi k n}{N}}, \quad 0 \le n \le N-1 \tag{16}$$

where $Z_k = Z_{N-k}^*, 0 < k < N/2$. The asymmetric clipping of z_n are subsequently performed to obtain the non-negative signal $z_{n,ACO}$, which is expressed as

$$z_{n,ACO} = \begin{cases} z_n, & z_n \ge 0 \\ 0, & z_n < 0 \end{cases} \tag{17}$$

Finally, the EEADO-OFDM obtain a superposition signal by imposing the clipped signal of ACO-OFDM $z_{n,ACO}$ and DCO-OFDM signal $v_{n,DCO}$ as follows

$$t_{n,EEADO} = z_{n,ACO} + v_{n,DCO}, \quad 0 \le n \le N-1 \tag{18}$$

Similar to (8), the EEADO-OFDM signal with the LED nonlinearity can be expressed as

$$t_{n,EEADO}^{clip} = \begin{cases} \varepsilon_{upper}, & t_{n,EEADO} > \varepsilon_{upper}, \\ t_{n,EEADO}, & 0 \le t_{n,EEADO} \le \varepsilon_{upper}, \\ 0, & t_{n,EEADO} < 0, \end{cases} \tag{19}$$

B. The Block Diagram of EEADO-OFDM Receiver

The EEADO-OFDM receiver block diagram is illustrated in Fig. 2. The proposed receiver is nearly identical to that of the conventional ADO-OFDM system, differing only in the interference cancellation process specific to the DCO-OFDM branch. The electrical signal r_n from the photodiode passes through the process of removing the cyclic prefix, where perfect synchronization is assumed. After the operation of N-point FFT, the frequency-domain signal R_k is given by.

$$R_k = \frac{1}{\sqrt{N}} \sum_{n=0}^{N-1} r_n e^{-j\frac{2\pi k n}{N}}, \quad 0 \le k \le N-1 \tag{20}$$

According to [5], it is established that the noise introduced during the clipping operation in conventional ACO-OFDM systems does not interfere with the original transmitted signal. Because the proposed EEADO-OFDM has the same ACO-OFDM branch

as that of ADO-OFDM, the ACO-OFDM symbols allocated on the odd subcarriers in EEADO-OFDM can be estimated as follows [20]

$$\tilde{Y}_k = \arg \min_{Y_k \in M_o} \left\| \frac{2R_k}{H_k} - Y_k \right\|^2, \tag{21}$$

where $k = 2N_{int}+1, 2N_{int}+3, \ldots, N/2-1$, M_o is the constellation sizes of the ACO-OFDM symbols allocated to odd subcarriers and the estimation of the channel frequency response H_k is perfectly known at the receiver. Moreover, the multiplication by 2 is used to compensate the clipping effect. The interference transmitted on the odd subcarriers can be directly obtained from R_k as follows [20]

$$\tilde{S}_k = 2R_k/H_k, \tag{22}$$

where $k = 1, 3, \ldots, 2N_{int}-1$. The time-domain regenerated signal $\tilde{z}_{n,ACO}$ can be obtained by $\tilde{Y}_k$ and $\tilde{S}_k$ with the sequential operations of FFT and asymmetric clipping, which are given by (16) and (17), respectively. After subtracting $\tilde{z}_{n,ACO}$ from the received time-domain signal, DCO-OFDM signals are obtained as

$$\tilde{v}_{n,DCO} = r_n - \tilde{z}_{n,ACO} = x_n + s_n + e_n + w_n, \tag{23}$$

where $e_n = z_{n,ACO} - \tilde{z}_{n,ACO}$ is the estimation error from the ACO-OFDM symbol estimation and w_n is the AWGN noise. Then, the frequency-domain DCO-OFDM signals on the even subcarriers can be obtained by applying the N-point FFT operation on (23) as follows

$$\tilde{V}_{k,DCO} = X_k + S_k + E_k + W_k, k \in \text{even} \tag{24}$$

where E_k is the frequency-domain component of e_n. At high SNR, indicating $E_k \approx 0$ and $\tilde{S}_k = S_k$, the estimated interference $\tilde{S}_k$ will be subtracted from $\tilde{V}_{k,DCO}$ to successfully estimate the DCO-OFDM symbols as follows

$$\tilde{X}_k = \arg \min_{X_k \in M_e} \|\tilde{V}_{k,DCO} - \tilde{S}_k - X_k\|^2, k \in \text{even} \tag{25}$$

where M_e is the constellation sizes of the DCO-OFDM symbols allocated to even subcarriers.

IV. The Properties Analysis of the EEADO-OFDM Systems

In this section, the numerical analysis of computational complexity, bit error error, optical power and spectral efficiency for the EEADO-OFDM systems are presented.

A. Computational Complexity

As can be seen in Fig. 1, the transmitter of the EEADO-OFDM systems require two N-point IFFT and one N-point FFT blocks, indicating that the computational complexity of transmitter can be calculated by $3\mathcal{O}(N \log N)$. Similarly, the receiver of the EEADO-OFDM systems require two N-point FFT and one N-point IFFT operations, indicating that the receiver has the computational complexity of $3\mathcal{O}(N \log N)$. For ADO-OFDM systems [17], the transmitter requires two N-point FFT operations and the receiver requires two N-point FFT and two N-point IFFT operations. Thus, the computational complexity of transmitter and receiver can be calculated by $2\mathcal{O}(N \log N)$ and $4\mathcal{O}(N \log N)$, respectively. Evidently, the analysis shows that EEADO-OFDM and ADO-OFDM have the same computational complexity of the required IFFT and FFT blocks. Although the total computational complexity of EEADO-OFDM is slightly higher than ADO-OFDM due to the extra operations of bias calculations and interference cancellation, it is acceptable considering the improvement of BER.

B. BER

Since the introduced bias s_n does not interfere with the ACO-OFDM symbols at odd subcarriers, the BER of ACO-OFDM in EEADO-OFDM is equal to that of ACO-OFDM in conventional ADO-OFDM, which can be formulated as follows [21]:

$$P_{b,ACO} = \frac{2(\sqrt{M_o}-1)}{\sqrt{M_o}\log_2(M_o)} \text{erfc}\left[\sqrt{\frac{3}{2}\cdot\frac{SNR}{M_o-1}}\right] \tag{26}$$

where $\text{erfc}[x] = \frac{2}{\sqrt{\pi}}\int_x^\infty e^{-t^2}dt$ represents the complementary error function and SNR is the abbreviation of the signal-to-noise ratio which is defined as $SNR = E_s/N_0$. E_s and N_0 denote the electrical energy per symbol and the power spectral density of the noise, respectively.

Then, the BER performance of the DCO-OFDM in EEADO-OFDM is derived as follows:

$$\begin{aligned} P_{b,DCO} &= P_{b,ACO}\cdot P_{b,F} + (1-P_{b,ACO})\cdot P_{b,D} \\ &= P_{b,D} + P_{b,ACO}(P_{b,F} - P_{b,D}) \end{aligned} \tag{27}$$

where $P_{b,F}$ denotes the BER of the DCO-OFDM given that the ACO-OFDM symbols are not decoded correctly and $P_{b,D}$ is the BER of DCO-OFDM when ACO-OFDM symbols are decoded correctly. At high SNR, indicating that $P_{b,ACO} \approx 0$, (27) can be further derived as follows

$$\begin{aligned} P_{b,DCO} &\simeq P_{b,D} \\ &= \frac{2(\sqrt{M_e}-1)}{\sqrt{M_e}\log_2(M_e)} \text{erfc}\left[\sqrt{\frac{3}{2}\cdot\frac{SNR}{M_e-1}}\right] \end{aligned} \tag{28}$$

Notice that (26) and (28) are only suitable for square QAM. The overall average BER performance is derived as

$$P_{b,EEADO} = \frac{(\frac{N}{4}-N_{int})\log_2 M_o \cdot P_{b,ACO} + (\frac{N}{4}-1)\log_2 M_e \cdot P_{b,DCO}}{(\frac{N}{4}-N_{int})\log_2 M_o + (\frac{N}{4}-1)\log_2 M_e} \tag{29}$$

C. Optical Power

In conventional ADO-OFDM, a constant DC bias $B_{DC,DCO}$ is added to DCO-OFDM branch in ADO-OFDM, indicating that the average optical power of ADO-OFDM signal is calculated by

$$\begin{aligned} P_{o,ADO} &= E[t_{n,ADO}] \\ &= E[y_{n,ACO}] + E[x_{n,DCO}] \\ &= \frac{\sigma_Y}{2\sqrt{\pi}} + B_{DC,DCO} \end{aligned} \tag{30}$$

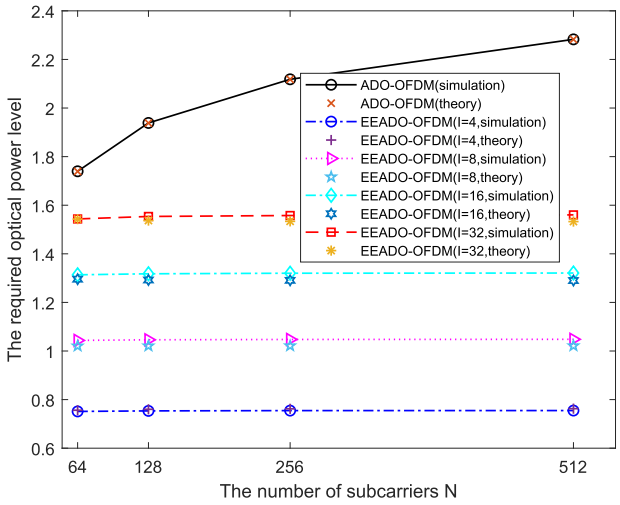

Fig. 3. Required optical power to obtain the unipolar signals for the EEADO-OFDM and ADO-OFDM.

where the first term of last equal sign comes from the fact that the average optical power of ACO-OFDM branch derived in [5] and the second term of last equal sign because x_n has a zero mean. As given in (18), the average optical power of EEADO-OFDM signal is calculated by

$$\begin{aligned} P_{o,EEADO} &= E[t_{n,EEADO}] \\ &= E[z_{n,ACO}] + E[v_{n,DCO}] \\ &= E[z_{n,ACO}] + E[x_n] + E[s_n] \\ &= \frac{\sigma_Z}{2\sqrt{\pi}} + \underbrace{\frac{1}{G}\sum_{g=0}^{G-1} E[m_g]}_{\stackrel{\text{def}}{=} B_{DC,EEADO}} \end{aligned} \tag{31}$$

where the second term of last equal sign because the s_n has the period of G and $\sigma_Z = \sqrt{E[|Z_k|^2]}$ is the standard deviation of Z_k. From (31), it can be seen that the introduced bias in EEADO-OFDM can be calculated by $\frac{1}{G}\Sigma_{g=0}^{G-1}E[m_g]$, which highly depends on the values of m_g. As we know, the conventional ADO-OFDM transmission signals are given by (7). Because $y_{n,ACO} \geq 0$, $t_{n,ADO}$ may not be the unipolar signals when the added $B_{DC,DCO}$ is too small. In order to guarantee that ADO-OFDM signals have the unipolarity, the $B_{DC,DCO}$ is considered to be identical to absolute value of maximum negative peak of x_n. On the other hand, the proposed EEADO-OFDM signals always have the unipolarity due to the introduction of a time-domain sequence. As derived in (31), it can be seen that the required power level of EEADO-OFDM highly depends on the values of I. To guarantee that ADO-OFDM and EEADO-OFDM signals have the unipolarity, the required average optical power levels are provided in Fig. 3. In Fig. 3, 16-QAM for ACO-OFDM branch and 16-QAM for DCO-OFDM branch are adopted in both ADO-OFDM and EEADO-OFDM schemes. The size of IFFT is set to 64, 128, 256 and 512.

TABLE I
REQUIRED OPTICAL POWER TO ACHIEVE $P_{o,EEADO} \approx P_{o,ADO}$ FOR ADO-OFDM AND EEADO-OFDM

	N=128	$P_{o,EEADO}$	$P_{o,ADO}$	$B_{DC,DCO}$
Case I	I=4,G=32	0.65	0.65	0.25 dB
Case II	I=8,G=16	1.05	1.05	3.10 dB
Case III	I=16,G=8	1.32	1.32	4.95 dB
Case IV	I=32,G=4	1.55	1.55	6.33 dB

It can be observed that the required average optical power of EEADO-OFDM is much lower than that of ADO-OFDM in any case, which means that EEADO-OFDM has the higher power efficiency. Another observation is that the required average optical power of ADO-OFDM slightly increases with the number of subcarrier while the required average optical power of EEADO-OFDM are almost identical for any N. Nevertheless, the required average optical power of EEADO-OFDM increases proportionally with the number of subblocks I. Finally, the simulation results provided in Fig. 3 are also consistent with the theoretical analysis defined by (30) and (31) for ADO-OFDM and EEADO-OFDM, respectively.

Generally, the average illumination level of LED output is defined as the average optical power in OWC systems. To achieve the same average illumination level for both ADO-OFDM and EEADO-OFDM systems, we further study the required average optical power to achieve $P_{o,EEADO} \approx P_{o,ADO}$. Because the optical power of EEADO-OFDM highly depends on the number of subblocks I, we firstly obtained the $P_{o,EEADO}$ for different subblocks I and the simulation results are provided in the third column of Table I, where the number of subblocks I for the case I, case II, case III and case IV is equal to 4, 8, 16, and 32, respectively. On the other hand, the required $B_{DC,DCO}$ of ADO-OFDM to achieve $P_{o,EEADO} \approx P_{o,ADO}$ are also simulated and provided in the last column of Table I. It can be seen that the required $B_{DC,DCO}$ in (30) are 0.25 dB, 3.10 dB, 4.95 dB, 6.32 dB for case I, case II, case III, and case IV of EEADO-OFDM, respectively.

D. Spectral Efficiency

For EEADO-OFDM systems, there are $N/4 - N_{int}$ and $N/4 - 1$ effective subcarriers for ACO-OFDM branch and DCO-OFDM branch, respectively. Considering the length of cyclic prefix N_{cp}, the spectral efficiency for EEADO-OFDM is given by

$$\Phi_{EEADO} = \frac{(\frac{N}{4} - N_{int})\log_2 M_o}{N + N_{cp}} + \frac{(\frac{N}{4} - 1)\log_2 M_e}{N + N_{cp}} \tag{32}$$

where M_e and M_o represent two constellation sizes used in even and odd subcarriers of EEADO-OFDM systems. Obviously, when N is much larger than N_{cp} and the same constellation alphabets are adopted on odd and even subcarriers (i.e. $M_o = M_e = M$), the corresponding approximation of spectrum efficiency for EEADO-OFDM is calculated as

$$\Phi_{EEADO} \approx \frac{1}{2}\log_2 M - \frac{1}{2I}\log_2 M \tag{33}$$

TABLE II
SPECTRAL EFFICIENCY COMPARISON BETWEEN EEADO-OFDM AND ADO-OFDM

constellation sizes (odd - even)	Φ_{EEADO}	Φ_{ADO}
16QAM-16QAM	Case I, Φ_{EEADO} =1.5	2
	Case II, Φ_{EEADO} =1.75	
	Case III, Φ_{EEADO} =1.87	
	Case IV, Φ_{EEADO} =1.93	
64QAM-64QAM	Case I, Φ_{EEADO} =2.25	3
	Case II, Φ_{EEADO} =2.62	
	Case III, Φ_{EEADO} =2.81	
	Case IV, Φ_{EEADO} =2.91	
128QAM-128QAM	Case I, Φ_{EEADO} =2.62	3.5
	Case II, Φ_{EEADO} =3.06	
	Case III, Φ_{EEADO} =3.28	
	Case IV, Φ_{EEADO} =3.39	
256QAM-256QAM	Case I, Φ_{EEADO} =3	4
	Case II, Φ_{EEADO} =3.5	
	Case III, Φ_{EEADO} =3.75	
	Case IV, Φ_{EEADO} =3.875	

Similarly, the spectral efficiency for ADO-OFDM is given by

$$\Phi_{ADO} = \frac{N(\log_2 M_o + \log_2 M_e)}{4(N+N_{cp})} - \frac{\log_2 M_e}{N+N_{cp}} \approx \frac{1}{2}\log_2 M \tag{34}$$

As derived in (33) and (34), the spectrum efficiency of ADO-OFDM is only associated with the adopted constellation sizes while the spectrum efficiency of EEADO-OFDM is associated with the adopted constellation sizes and the number of subblocks I. To assure that parameters consistency, the four cases defined in Table II are identical to that of Table I, which means that the number of subblocks I for the case I, case II, case III and case IV is equal to 4, 8, 16, and 32, respectively. Upon observing Table II, the spectrum efficiency of EEADO-OFDM for each case is lower than that of ADO-OFDM with the same constellation sizes due to the some odd carriers are preserved for the transmissions of the interference caused from the s_n. However, when I increases, the spectrum efficiency of EEADO-OFDM approaches to that of ADO-OFDM for different combination of constellation sizes. Moreover, we can also see from the results of Table II, the spectrum efficiency of EEADO-OFDM for smaller I approximates to that of ADO-OFDM by increasing the modulation order.

For example, at the case I, EEADO-OFDM with the combination of 256 QAM and 256 QAM has the approximate spectrum efficiency to that of ADO-OFDM with the combination of 64 QAM and 64 QAM. For the case II, EEADO-OFDM with the combination of 256 QAM and 256 QAM has the approximate spectrum efficiency to that of ADO-OFDM with the combination of 128 QAM and 128 QAM. Although the spectrum efficiency of EEADO-OFDM for smaller I is lower than that of ADO-OFDM, it is acceptable considering the improvement of BER, which is provided in the following section.

V. SIMULATION RESULTS

With the same receiver architecture for ACO-OFDM branch, it is evident that BER of ACO-OFDM branch for both systems are identical. We only evaluate the overall average BER performances of EEADO-OFDM and ADO-OFDM systems through simulations in this work. Three scenarios are considered, each with the same average illumination level, spectrum efficiency, and non-linear LED transmission. The simulation involves a total of 10^6 OFDM symbols, a cyclic prefix length of 16, and an IFFT size of $N = 128$. Additionally, both systems assume equal optical power allocation between the ACO-OFDM branch and the DCO-OFDM branch.

The line-of-sight (LoS) channel adopted in this paper is expressed as follows [22]

$$h_{LoS} = \frac{(m+1)A}{2\pi d^2}\cos^m(\phi)\cos(\psi) \tag{35}$$

where ϕ and ψ denote the irradiance angle of the LED and the incidence angle of the photodiode, respectively; $m = -\ln(2)/\ln(\cos(\phi_{1/2}))$ denotes the Lambert order with half-power semi-angle of LED $\phi_{1/2}$; A is the detection area of the photodiode; and d is the Euclidean distance between the transmitter and the receiver. The parameters mentioned above are identical to those in [22]. In addition, perfect channel equalization is assumed and the constraints related to bandwidth in OWC systems were not discussed in this work due to our work focus on the single-user scenario and the need for brevity.

A. The Same Average Illumination Level

The BER performance comparisons between the ADO-OFDM and EEADO-OFDM systems under the condition of the same average illumination level are firstly considered. As discussed in Section IV-C, the required $B_{DC,DCO}$ of ADO-OFDM to achieve same average illumination level as EEADO-OFDM with four cases have been provided in Table I. With these configuration parameters, the corresponding BER performance comparisons between the ADO-OFDM and EEADO-OFDM with four cases are given from Figs. 4 to 7. It is clearly observed from Figs. 4 to 6 that ADO-OFDM systems with different constellation groups always exhibit the BER error floors even increasing the SNR. Moreover, one can clearly observe from Fig. 7 that the BER error floor of ADO-OFDM with 16-QAM modulation no longer exhibits. However, ADO-OFDM still exhibits the BER error floors for higher constellation groups such as 64-QAM, 128-QAM, and 256-QAM observing from Fig. 7. As can be seen from Figs. 4 to 7, it is evident that the EEADO-OFDM exhibits no error floors of BER at the cases of higher constellation groups. This is because clipping noise is not introduced in the DCO-OFDM branch of the EEADO-OFDM system.

B. The Same Spectrum Efficiency

The BER performance comparisons between the ADO-OFDM and EEADO-OFDM systems under the condition of the same spectrum efficiency are further considered in this subsection. As shown in Table II, the same spectrum efficiency

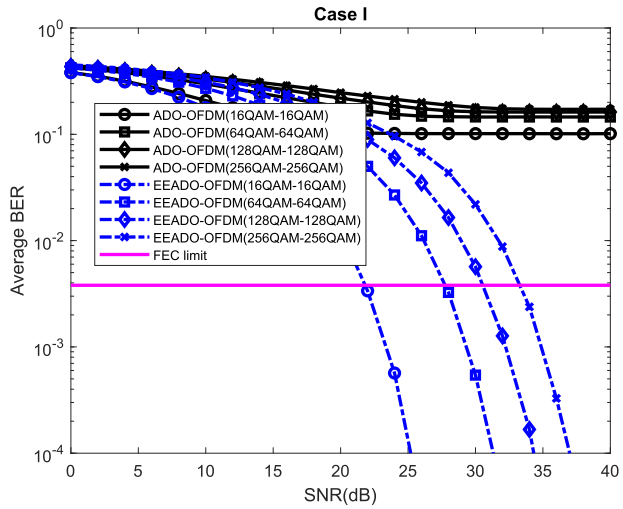

Fig. 4. Comparison of BER performance between the EEADO-OFDM and ADO-OFDM under the condition of the same average illumination level (Case I).

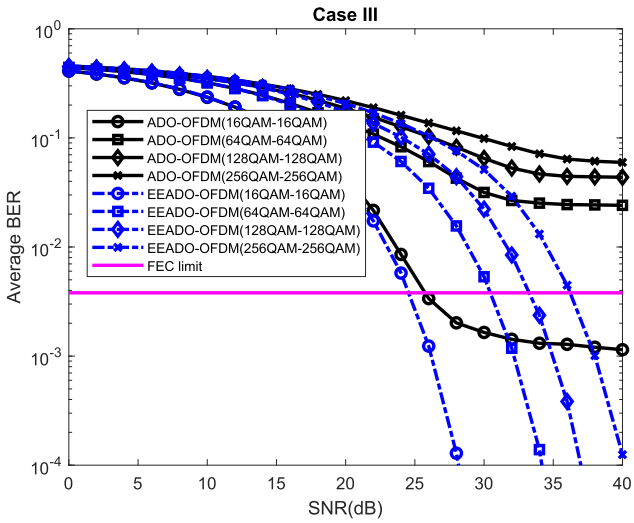

Fig. 6. Comparison of BER performance between the EEADO-OFDM and ADO-OFDM under the condition of the same average illumination level (Case III).

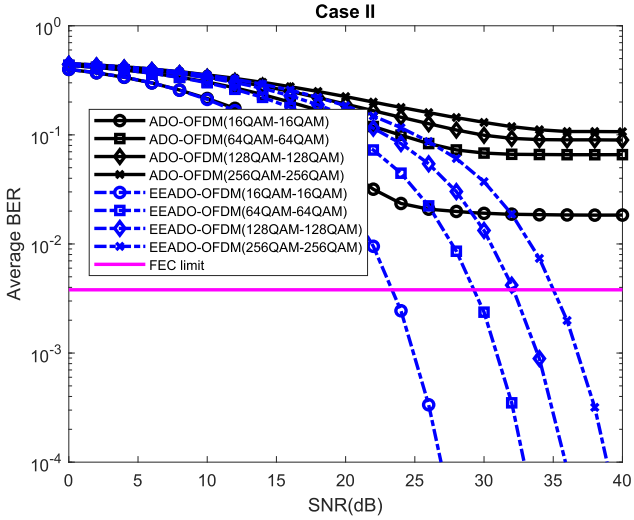

Fig. 5. Comparison of BER performance between the EEADO-OFDM and ADO-OFDM under the condition of the same average illumination level (Case II).

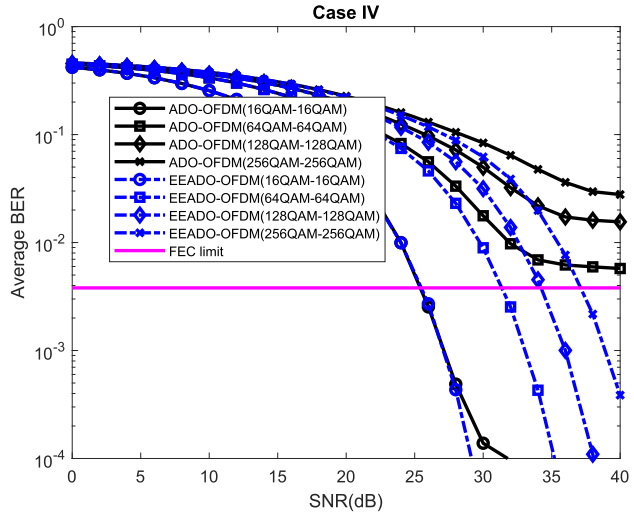

Fig. 7. Comparison of BER performance between the EEADO-OFDM and ADO-OFDM under the condition of the same average illumination level (Case IV).

can be achieved through two possibilities. The first possibility occurs when the spectrum efficiency is 3, and the other possibility occurs when the spectrum efficiency is 3.5. For a spectrum efficiency of 3, the ADO-OFDM system utilizes 64-QAM constellation sizes, while the EEADO-OFDM system employs 256-QAM constellation sizes under configuration of case I. When the spectrum efficiency is 3.5, the ADO-OFDM system switches to 128-QAM constellation sizes, and the EEADO-OFDM system continues to use 256-QAM constellation sizes under configuration of case II. Using the parameters mentioned above, Fig. 8 illustrates a comparison of BER performance between EEADO-OFDM and ADO-OFDM systems operating at the same spectrum efficiency. The graph clearly shows that EEADO-OFDM outperforms ADO-OFDM by significantly reducing BER. This suggests that EEADO-OFDM has a superior capability to resist clipping noise at same spectrum efficiency levels when compared to ADO-OFDM.

C. Non-Linear LED Transmission

In order to meet the actual LED transmission, two upper clipping level $\varepsilon_{upper} = 4$ and $\varepsilon_{upper} = 4.5$ for EEADO-OFDM and ADO-OFDM systems are considered to determine the effects of LED nonlinearity on average BER performance as illustrated in Figs. 9 and 10. In both figures, the adopted constellation sizes for 16-QAM modulations. We observe the BER performance of EEADO-OFDM is still superior to ADO-OFDM under the

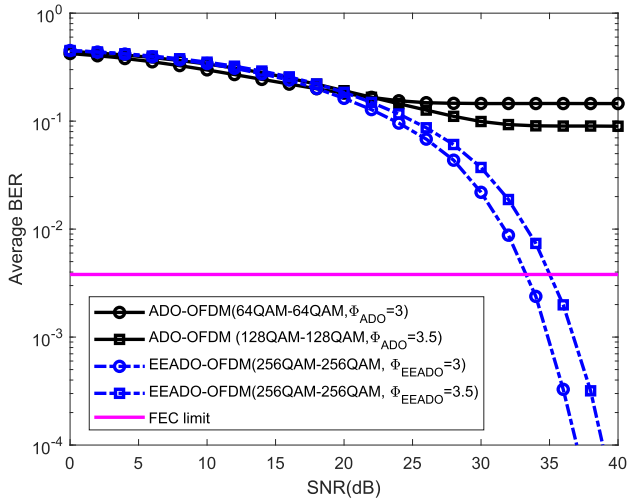

Fig. 8. Comparison of BER performance between the EEADO-OFDM and ADO-OFDM under the same spectrum efficiency.

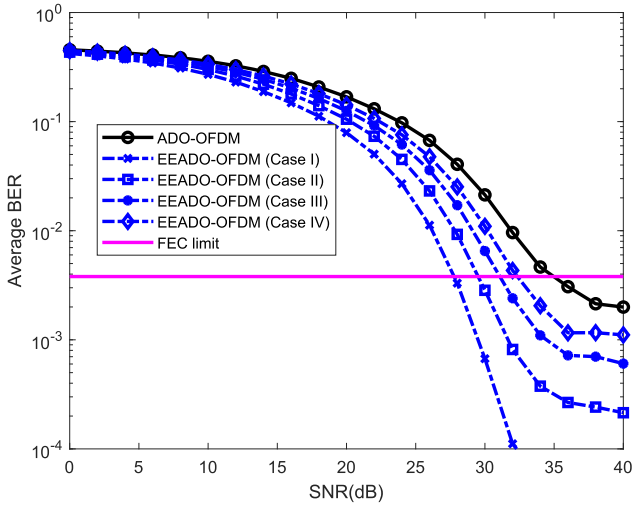

Fig. 9. Comparison of BER performance between EEADO-OFDM and ADO-OFDM under the condition of non-ideal LED transmission($\varepsilon_{upper} = 4.5$).

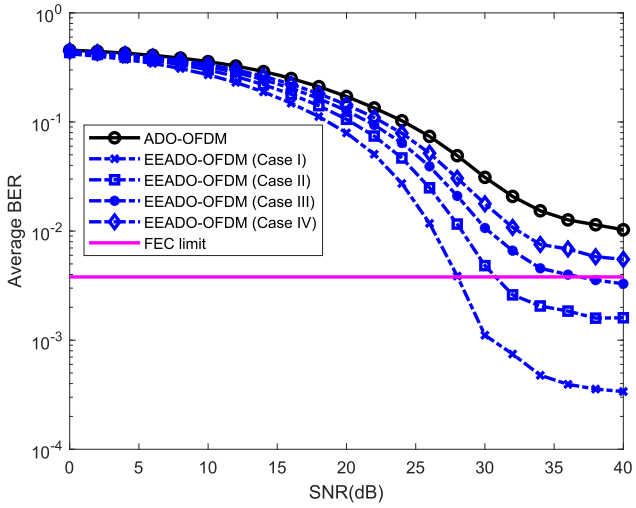

Fig. 10. Comparison of BER performance between EEADO-OFDM and ADO-OFDM under the condition of non-ideal LED transmission($\varepsilon_{upper} = 4$).

non-linear LED transmission. This is because EEADO-OFDM has the lower optical power level to obtain the unipolar signals. Moreover, the BER performance of EEADO-OFDM becomes worse with the increase of I. This is because the required average optical power of EEADO-OFDM increases proportionally with the number of subblocks I as demonstrated in Fig. 3.

VI. Conclusion

This paper introduces an EEADO-OFDM scheme, where the fixed DC bias of the DCO-OFDM branch is replaced with an adaptive DC bias. Compared to conventional ADO-OFDM, EEADO-OFDM significantly enhances the BER performance, especially in scenarios with low DC bias or higher modulation schemes. Additionally, it is demonstrated that EEADO-OFDM requires a substantially lower average optical power to maintain non-negative signals compared to ADO-OFDM in any situation. This indicates that EEADO-OFDM achieves higher power efficiency.

Appendix
Proof of S_k

By applying N-point FFT operation on (11), the k-th frequency-domain element is given by

$$S_k = \frac{1}{\sqrt{N}} \sum_{n=0}^{N-1} s_n e^{-j\frac{2\pi kn}{N}}, 0 \le k \le N-1 \tag{36}$$

With the property of (13), (36) is further expressed as

$$\begin{aligned} S_k &= \frac{1}{\sqrt{N}} \sum_{g=0}^{G-1} \Big[m_g e^{-j\frac{2\pi gk}{N}} + m_{g+G} e^{-j\frac{2\pi (g+G)k}{N}} \\ &\quad + m_{g+2G} e^{-j\frac{2\pi (g+2G)k}{N}} + \cdots + m_{g+(I-1)G} e^{-j\frac{2\pi [g+(I-1)G]k}{N}} \Big] \\ &= \frac{1}{\sqrt{N}} \sum_{g=0}^{G-1} m_g e^{-j\frac{2\pi gk}{N}} \left(1 + e^{-j\frac{2\pi Gk}{N}} + \cdots + e^{-j\frac{2\pi (I-1)Gk}{N}} \right) \\ &= \frac{1}{\sqrt{N}} \sum_{g=0}^{G-1} m_g e^{-j\frac{2\pi gk}{N}} \left(1 + e^{-j\frac{2\pi k}{I}} + \cdots + e^{-j\frac{2\pi (I-1)k}{I}} \right) \\ &= \frac{1}{\sqrt{N}} \sum_{g=0}^{G-1} m_g e^{-j\frac{2\pi gk}{N}} \frac{1-e^{-j2\pi k}}{1-e^{-j\frac{2\pi k}{I}}} \end{aligned} \tag{37}$$

where the last equal sign is generated from the sum of geometric sequence. When k is odd, where $e^{-j2\pi k} = 1$, we have $S_k = 0$ for odd k. On the other hand, if k is even value which satisfies with $k = I \cdot t$ for $0 \le t \le N/I - 1$, (36) is expressed as

$$\begin{aligned} S_k &= \frac{1}{\sqrt{N}} \sum_{g=0}^{G-1} m_g e^{-j\frac{2\pi gIt}{N}} \left(1 + e^{-j2\pi t} + \cdots + e^{-j2\pi (I-1)t} \right) \\ &= \frac{I}{\sqrt{N}} \sum_{g=0}^{G-1} m_g e^{-j\frac{2\pi gIt}{G}}, k = I \cdot t \end{aligned} \tag{38}$$

If k is even value which satisfies with $k = It + 2l$ for $1 \leq l \leq I/2 - 1$, substituting $k = It + 2l$ into (36) yields the S_k as

$$S_k = \frac{1}{\sqrt{N}} \sum_{g=0}^{G-1} m_g e^{-j\frac{2\pi g(It+2\,l)}{N}} \frac{1 - e^{-j2\pi 2\,l}}{1 - e^{-j\frac{2\pi 2\,l}{I}}} = 0 \qquad (39)$$

REFERENCES

[1] J. Song, W. Ding, F. Yang, H. Yang, B. Yu, and H. Zhang, "An indoor broadband broadcasting system based on PLC and VLC," *IEEE Trans. Broadcast.*, vol. 61, no. 2, pp. 299–308, Jun. 2015.

[2] K. Ali et al., "Measurement campaign on 5G indoor millimeter wave and visible light communications multi component carrier system," *IEEE Trans. Broadcast.*, vol. 68, no. 1, pp. 156–170, Mar. 2022.

[3] P. H. Pathak, X. Feng, P. Hu, and P. Mohapatra, "Visible light communication, networking, and sensing: A survey, potential and challenges," *IEEE Commun. Surveys Tuts.*, vol. 17, no. 4, pp. 2047–2077, Fourth Quarter 2015.

[4] N. Fernando, Y. Hong, and E. Viterbo, "Flip-OFDM for unipolar communication systems," *IEEE Trans. Commun.*, vol. 60, no. 12, pp. 3726–3733, Dec. 2012.

[5] J. Armstrong and A. J. Lowery, "Power efficient optical OFDM," *Elect. Lett.*, vol. 42, no. 6, pp. 370–372, Mar. 2006.

[6] J. Lian and M. Brandt-Pearce, "Polarity-header optical OFDM for visible light communication systems," *IEEE Photon. J.*, vol. 11, no. 5, Oct. 2019, Art. no. 7906213.

[7] H. Elgala and T. D. C. Little, "Polar-based OFDM and SC-FDE links toward energy-efficiency Gbps transmission under IM-DD optical system constraints," *IEEE/OSA J. Opt. Commun. Netw.*, vol. 7, no. 2, pp. A277–A284, Feb. 2015.

[8] D. Tsonev, S. Sinanovic, and H. Haas, "Novel unipolar orthogonal frequency division multiplexing (U-OFDM) for optical wireless," in *Proc. IEEE Veh. Technol. Conf.*, 2012, pp. 1–5.

[9] Q. Wang, C. Qian, X. Guo, Z. Wang, D. G. Cunningham, and I. H. White, "Layered ACO-OFDM for intensity-modulated direct detection optical wireless transmission," *Opt. Exp.*, vol. 23, no. 9, pp. 12382–12393, May 2015.

[10] X. Zhang, Q. Wang, R. Zhang, S. Chen, and L. Hanzo, "Performance analysis of layered ACO-OFDM," *IEEE Access*, vol. 5, pp. 18366–18381, Sep. 2017.

[11] R. Bai, S. Hranilovic, and Z. Wang, "Low-complexity layered ACO-OFDM for power-efficient visible light communications," *IEEE Trans. Green Commun. Netw.*, vol. 6, no. 3, pp. 1780–1792, Sep. 2022.

[12] M. Zhang and Z. Zhang, "An optimum DC-Biasing for DCO-OFDM system," *IEEE Commun. Lett.*, vol. 18, no. 8, pp. 1351–1354, Aug. 2014.

[13] Y. Jiang, D. Sun, X. Zhu, T. Zhou, T. Wang, and S. Sun, "Robust frequency-domain timing offset estimation for DCO-OFDM systems," *IEEE Commun. Lett.*, vol. 26, no. 8, pp. 1603–1607, Jul. 2022.

[14] W. W. Hu, "PAPR reduction in DCO-OFDM visible light communication systems using optimized odd and even sequences combination," *IEEE Photon. J.*, vol. 11, no. 1, Feb. 2019, Art. no. 7901115.

[15] X. Ling, J. Wang, X. Liang, Z. Ding, and C. Zhao, "Offset and power optimization for DCO-OFDM in visible light communication systems," *IEEE Trans. Signal Process.*, vol. 64, no. 2, pp. 349–363, Jan. 2016.

[16] J. Armstrong and B. J. C. Schmidt, "Comparison of asymmetrically clipped optical OFDM and DC-biased optical OFDM in AWGN," *IEEE Commun. Lett.*, vol. 12, no. 5, pp. 343–345, May 2008.

[17] S. D. Dissanayake and J. Armstrong, "Comparison of ACO-OFDM, DCO-OFDM and ADO-OFDM in IM/DD systems," *J. Lightw. Technol.*, vol. 31, no. 7, pp. 1063–1072, Apr. 2013.

[18] X. Huang, F. Yang, C. Pan, and J. Song, "Pre-distorted enhanced ADO-OFDM for hybird VLC network: A mutual-interference-free approach," *IEEE Photon. J.*, vol. 12, no. 2, Apr. 2020, Art. no. 79001512.

[19] X. Huang, F. Yang, C. Pan, and J. Song, "Advanced ADO-OFDM with adaptive subcarrier assignment and optimized power allocation," *IEEE Wireless Commun. Lett.*, vol. 8, no. 4, pp. 1167–1170, Aug. 2019.

[20] X. Huang, F. Yang, X. Liu, H. Zhang, J. Ye, and J. Song, "Subcarrier and power allocations for dimmable enhanced ADO-OFDM iterative interference cancellation," *IEEE Access*, vol. 7, pp. 28422–28435, 2019.

[21] Q. Wang, Z. Wang, and L. Dai, "Iterative receiver for hybrid asymmetrically clipped optical OFDM," *J. Lightw. Technol.*, vol. 32, no. 22, pp. 4471–4477, Nov. 2014.

[22] T. Wan, F. Yang, L. Cheng, and J. Song, "Spectral-efficient generalized spatial modulation based hybrid dimming scheme with LACO-OFDM in VLC," *IEEE Access*, vol. 6, no. 1, pp. 41153–41162, Aug. 2018.